Slider-Lubricant Interactions at the Head-Disk Interface

Rohit P. Ambekar and David B. Bogy,
Computer Mechanics Laboratory,
5146 Etcheverry Hall
Department of Mechanical Engineering
University of California
Berkeley, CA 94720

Email: rohit@cml.me.berkeley.edu

Abstract

As the flying height reduces below 5nm, the effect of lubricant on the slider flying attitude is gaining importance. A slider, either flying or in partial contact with the disk, affects the lubricant, which in turn causes changes in the flying condition of the slider. To investigate this effect, the lubricant profile under a flying slider was obtained experimentally as well as calculated numerically. The profile was then put into the airbearing code CMLAir to find the change in slider flying attitude due to inclusion of lubricant at the head-disk interface. From the simulations it was observed that the flying attitude of the slider does not change significantly unless there is substantial lubricant depletion.

In addition, an experimental study of slider-lubricant interactions during partial contact has also been done. Due to small head-disk spacing, an intermittent contact between the slider and the disk during operation is unavoidable. In such an event, the slider affects the lubricant on the disk much more as compared to when it is flying. It was found that certain characteristics of the slider such as its roll and position of side rails affect the lubricant. Further, it was also observed that a slider in partial contact depletes, redistributes and modulates the lubricant.

Introduction:

In a Hard Disk Drive (HDD), there exist multiple layers on the magnetic disk. On top of the magnetic layer there is a hard diamond-like carbon (DLC) overcoat of about 1-2nm to protect the magnetic layer against head crashes and corrosion. On top of the DLC, there exists a molecularly thin (~0.5-1.5nm) lubricant layer to reduce the friction and wear at the head-disk interface (HDI).

In order to achieve the areal recording density of 1 Tb/in^2, the head-disk spacing has to be reduced to about 2.5 nm. At such a small spacing, the effect of lubricant needs to be considered in simulating the fly height of the slider. Various experimental studies [1-4] have been done to investigate lubricant changes under a flying slider and its effect on magnetic spacing. It has been reported that a flying slider modulates [2-3] and redistributes [1] the lubricant. Simulations [3] attribute the lubricant modulation to ABS shear effects. This lube modulation can prove detrimental to the dynamic performance of the slider. Further, the ABS air shear and pressure can also contribute to the displacement of the lubricant under the slider. Hence, even in static simulations, this effect needs to be considered in order to predict the correct fly height of the slider.

In this report we conducted both experimental and numerical studies of lubricant changes under an ABS. In the first section the lubricant distribution profiles under a flying slider were obtained experimentally as well as by conducting simulations. Subsequently, these profiles were included in the CMLAir static solver to estimate the flying attitude (fly height, pitch, roll, pressure distribution, etc) of the slider after inclusion of lubricant. Comparison of the flying attitudes with and without the inclusion of the lubricant is made and discussed.

In the second section an experimental study of slider-lubricant interactions in the partial contact regime is presented. As the slider flies in close proximity of the disk, intermittent contacts are unavoidable during operation of the HDD. Not much literature is available concerning how the lubricant is affected during these intermittent contacts as most effort is concentrated on slider-lubricant interactions in the non-contact regime. Hence, such a study is carried out to understand the effect of intermittent slider-disk contacts on the lubricant distribution.

Section I: Non-contact regime

Experiments

The Candela Optical Surface Analyzer (OSA) was used to experimentally measure the lubricant profile under a flying slider. OSA can measure the lubricant thickness with a sub-Å accuracy. Since the OSA gives an output in terms of percentage reflectivity (as measured by the ellipsometer in the OSA), a calibration of percentage reflectivity vs. lubricant thickness was done using ZDOL disks with three different lubricant thicknesses (Fig. 1) and the calibration constant was determined to be -0.076%/nm. Sliders of two different ABS designs (CML pico-7nm and CML femto-3.5nm) as shown in Fig. 2 were flown over disks with 1.2nm of Zdol lubricant on the OSA spinstand for 30 minutes. The linear velocities were 23.37 mps (7.2K rpm @ 31 mm) and 32.46 mps (10K rpm @ 31 mm) for the pico and femto sliders, respectively. The lubricant profile measurements were carried out in-situ. An acoustic emission sensor was used to detect slider-disk contact.

Scans were done after 0, 15 and 30 minutes for each slider-disk combination to confirm that the lubricant profile was reaching a steady state. A very high radial resolution (0.1μm) of scan on the OSA was used to measure the lubricant profile with sufficient accuracy. The angular resolution was 2048 points per track. Each scan furnished a two dimensional (radial x angular) reflectivity data. Averaging was done in the angular direction to obtain average percentage reflectivity as a function of radius. This was then converted into average lubricant thickness as a function of radius using the calibration curve. Multiple experiments were conducted for each slider design and the lubricant profile corresponding to maximum depletion was used in simulations for adding onto the slider ABS profile.

Simulations

A. Using lubricant profiles from experiments

The lubricant profiles obtained from experiments were used in the CMLAir static simulator to investigate changes in the slider flying attitude due to inclusion of the lubricant. The lubricant profile was mapped onto the existing grid on the slider made in CMLAir. Though the lubricant is on the disk, its profile was added to the slider profile and the disk was assumed flat (Fig.3). This was achieved by making suitable changes to the software. The newer versions of CMLAir (version 6.55 and later) have a suitable User Defined Geometry (UDG) option, which can be used to add the lubricant profile to the slider. Since the UDG assumes that the grid points are regularly spaced, a regular (non-adaptive) grid of 289x289 was used for meshing. Adding of lubricant profile to the slider does not change the physics of the problem as the gap height between the slider and the

disk remains constant at each grid point, whether the lubricant profile is added on the disk or the slider. Static simulations were carried out with and without adding the lubricant profile. The experimentally measured lubricant profile was assumed not to change due to ABS pressure.

B. Calculating the lubricant depletion profile

Using the 3-D Navier-Stokes equation, and setting the length scale in the thickness (Z) direction much less than in the lateral (X and Y) directions we can arrive at a lubricant thickness evolution equation considering lubricant flow due to ABS pressure as well as shear. Since the lubricant layer is molecularly thin there will also be velocity slip boundary conditions and existence of a Knudsen layer. Using a Couette flow profile due to shear and a Poiseuille flow profile due to pressure, we can arrive at the following continuum lubricant thickness evolution equation.

$$\frac{\partial h}{\partial t} = \frac{\partial (J_x)}{\partial x} + \frac{\partial (J_y)}{\partial y} \qquad \text{… continuity equation} \qquad (1)$$

where,

$$J_x = \frac{1}{\mu} \frac{\partial \left(p_{ABS} + p_{dis} \right)}{\partial x} \left(\frac{h^3}{6} + \Phi \right) + \frac{\tau_x}{\mu} \left(\frac{h^2}{2} \right) \qquad (2)$$

$$J_y = \frac{1}{\mu} \frac{\partial \left(p_{ABS} + p_{dis} \right)}{\partial y} \left(\frac{h^3}{6} + \Phi \right) + \frac{\tau_y}{\mu} \left(\frac{h^2}{2} \right) \qquad (3)$$

$$\Phi = \left(2 - \sigma_v \right) / \sigma_v * Kn \qquad (4)$$

Here,

h = h(x,y,t) = lubricant film thickness

J_x, J_y = flux in X and Y directions, respectively

μ = viscosity of the lubricant film (different from bulk viscosity [5] and strain-rate dependent, since the lubricant is a non-Newtonian fluid)

τ_x, τ_y = shear stress in the X and Y directions, respectively

σ_v = tangential momentum accommodation coefficient, and

Kn = Knudsen number

p_{dis} = disjoining pressure of the lubricant

p_{ABS} = airbearing pressure from CMLAir

From experimental evidence (Fig. 5), we see that the lubricant depletion profile is almost uniform in the x (circumferential) direction. The non-uniformity seen is thought to be due to disk runout and other externalities. The profile such as in Fig. 5 was seen when there was lubricant transfer to the slider or in some cases to some other part of the track, due to which the final lubricant volume was not equal to the initial lubricant volume in that part on the disk. However, after initial loss in lubricant volume, there was no more lubricant transfer due to which the lubricant volume was conserved.

Thus equation (1) can still be applied to determine the steady-state solution. Under steady-state, the LHS of equation (1) is zero at every point (x,y) in the domain. Due to the uniformity of the lubricant profile in the angular direction, it is reasonable to assume that there is no flow of lubricant in this direction in steady-state. Thus $\partial J_x / \partial x = 0$ and to satisfy the equation (1) we must require $\partial J_y / \partial y = 0$. For 0° skew, we have $\tau_y \approx 0$ which leaves us to satisfy $\partial\left(p_{ABS} + p_{dis}\right)/\partial y = 0$ in order to satisfy the steady-state condition. This is satisfied by $p_{dis} + p_{ABS} = Const$ and this was used to determine the steady-state lubricant depletion due to the flying slider under the above conditions.

The disjoining pressure p_{dis}, is defined as the negative gradient of the surface energy with respect to the film thickness [6,7]. Since the lubricant on the disk is molecularly thin its surface energy is a strong function of its film thickness and the surface energy of the substrate below, which is the carbon overcoat (COC). Thus, the disjoining pressure is non-zero and significant, especially for our thickness range of the lubricant (0-2nm). Just as for the surface energy, the disjoining pressure has two components: dispersive and polar [7]. The dispersive component is a result of the van der waals forces and the polar part is a result of polar interactions. The relations can be written as:

$$p^{d}_{dis} = -\frac{d\gamma^{d}}{dh} = \frac{A}{6\pi h^{3}}; \tag{5}$$

$$p^{p}_{dis} = -\frac{d\gamma^{p}}{dh} = -\frac{\left(\sum_{i=1}^{k} a_i h^{i}\right)}{dh} \tag{6}$$

where $()^{d}$ is the dispersive component, $()^{p}$ is the polar component and γ is the surface energy. It has been shown that the dispersive disjoining pressure can be written in terms of the film thickness h and the Hamaker constant A [6-8]. By comparison, there is no established relation between the polar component with the film thickness, and so a polynomial fit (coefficients a_i) of the film thickness h is used to fit the experimentally measured polar surface energy [7].

Various studies have measured the total (dispersive + polar) surface energy/ disjoining pressure of ZDOL. Fukuzawa et. al. [9] determined the disjoining pressure for PFPE 4000 using fabricated microgrooves (Fig. 6(a)). Waltman et. al. [10] determined the dispersive and polar surface energies of Zdol (Fig. 7(a)), while Smallen et. al. [11]

determined the total disjoining pressure of AM3001 as a function of lubricant thickness. Suitable curve fits to these experimentally measured disjoining pressures are shown in Figs. 6(a) and 8(a), and the resulting fit equations for dispersive and polar surface energies as shown in Fig.7(a-b) were differentiated to obtain the corresponding disjoining pressure (Fig. 7(c)). The fits shown in Figs. 6(a) and 7(c) are henceforth referred to as models 1 and 2, respectively. Similarly, the fits corresponding to thin line and thick line in 8(a) are referred to as models 3A and 3B respectively.

The pressure profile of the CML-7nm slider is used to illustrate the resultant lubricant profiles predicted by each surface energy measurement using $p_{dis} + p_{ABS} = Const$. The condition of volume conservation of lubricant was not imposed while solving for lubricant depletion as it was not observed experimentally in the absence of lubricant modulation. A single curve fit for the disjoining pressure enabled us to obtain the film thickness *h* without an iterative procedure when models 1, 3A and 3B were used. However, an iterative procedure had to be used to obtain *h* with model 2. The resultant lubricant profiles for the cases of 1.0 nm and 2.0 nm lubricant thickness are shown next to each of the models (Figs. 6-8). In all of the simulations the disk as assumed to be smooth (no asperities and roughness) and no contact model was used.

As mentioned before, it was seen experimentally that the lubricant depletion profile was uniform in the circumferential direction in absence of lubricant modulation (Fig. 5). Hence, the lubricant profiles obtained from the above calculations were modified as shown in Fig. 9 to closely resemble the experimentally observed ones. The peak pressures corresponding to the width (y) direction were dragged/extruded along the x-direction to form a pressure envelope since the high pressure areas along the slider width

are assumed to be responsible for the lubricant depletion. The final lubricant profile obtained satisfies $\partial\left(p_{ABS(peak)} + p_{dis}\right)/\partial y = 0$, where $p_{ABS(peak)}$ is the peak ABS pressure along the slider width.

C. Using calculated lubricant profiles

The lubricant profile obtained above was then added to the slider profile and static FH simulations were conducted. It was observed that there was a change in the pressure distribution due to the presence of the lubricant profile. The change in the pressure distribution in turn affects the lubricant profile, although the change is not very significant. In order to obtain the exact pressure and lubricant profiles an iterative procedure, as shown in Fig. 10, was used. This procedure was tested for convergence, and Figs. 11(a) and (b) show the convergence results for the CML Pico and Femto sliders, respectively, using model 2 to calculate the lubricant depletion. This simulation procedure was then used on multiple ABS designs shown in Fig. 12 to study their effect on lubricant depletion and the change in their flying attitude due to the inclusion of the lubricant.

Results:

A. Experimental lubricant depletion profile

When the experiments were conducted to determine the lubricant depletion, lubricant modulation was observed in some cases. However, since this phenomenon is dynamic and cannot be modeled in static simulations, only the profiles which showed less or no modulations were considered for simulations. In the absence of modulations it was seen that the lubricant profile was uniform in the circumferential direction as shown in

Fig. 5 (the non-uniformity seen is thought to be an effect of disk runout). Hence, the lubricant profile was averaged in the circumferential direction without losing much information. Such averaged lubricant profile cross-sections have been plotted for the femto slider in Figs. 4(a-b). The lubricant had achieved steady-state depletion as there was not much change in the lubricant profiles between scans taken after 15 and 30 minutes after the start of tests. It is seen from the Figs. 4(a-b) that the lubricant depletion occurs primarily below the trailing pad where the airbearing pressure and shear are the maximum. Fig.4(c) shows the smoothed version of Fig. 4(b), while Fig. 4(d) is the smoothed version for the CML Pico slider. These lubricant profiles were added to the corresponding slider profiles and simulations were carried out according to the procedure outlined in the previous section.

B. Numerical lubricant depletion profile

Different models were used for calculating the lubricant depletion profiles, and the results are shown in Figs. 6-8. Further, the maximum and minimum height in each of the calculated lubricant profiles is shown in Table 1. In these simulations the CML Pico slider pressure profile was used. To simulate excessive lubricant depletion, we divided by 10 the slope of the disjoining pressure in model 3B, and the results are also included in Table 1 as model 3B/10. From the simulation procedure used it can be seen that the amount of lubricant depletion or buildup calculated by a model depends on the slope of disjoining pressure. From the table and the figures we see that model 1 overpredicts the lube buildup when thicker lubricant is used. This is because the slope of the corresponding disjoining pressure curve is very small as the lubricant thickness increases, which is always characteristic of a dispersive disjoining pressure. Hence, it is the polar

disjoining pressure that restricts the lubricant buildup for higher lubricant thicknesses as shown by the model 2 results. We also note that the slope of the disjoining pressure in model 2 is not constant over all lubricant thicknesses unlike models 3A and 3B. It predicts more depletion for higher lubricant thicknesses (agrees with experiments), while 3A and 3B predict constant depletion. From these characteristics we conclude that model 2 is the most physical model. However, the lubricant height h has to be solved iteratively while using model 2 unlike for the other models, and thus it takes more computational time.

Further, the experiments were also done with Zdol 4000 lubricant which allowed direct comparison between experimental and numerical lubricant profiles (Fig.13). It is seen that the model overpredicted the lubricant depletion for the CML pico as well as the femto designs. However, the experimental profiles show a wider valley compared to the calculated ones.

C. Comparison of flying attitudes with and without the inclusion of lubricant

Table 2 shows the flying attitude without the inclusion of lubricant (before) and with the inclusion of the experimental and calculated profiles. No significant change is seen in the flying attitude of the slider. This is primarily because of the small amount of lubricant depletion. To see the effect of a larger depletion in the flying attitude, we used model 3B/10 with various ABS designs (shown in Fig.12). The results are shown in Table 3. It is seen that under severe lubricant depletion the flying height drops by 0.1-0.2 nm. Further, the pitch increases slightly in four out of five cases. There is also an increase in pressure of as much as 0.52 atm in the case of the DSI femto slider, while the other designs display only a slight increase.

Discussion:

From the above experiments and simulations we find that the inclusion of the lubricant in static simulations yields only small changes in the flying characteristics of the slider. It should be noted that the modeling of lubricant depletion used in these simulations is too simplistic for explaining more complex slider-lubricant interactions. However, we see that the lubricant depletion obtained by simulations is of the same order of magnitude as the experimental data. The simple lubricant depletion model seems to fit certain experimental observations better (Fig. 13(c)), while it is unable to explain others in which there is some lubricant buildup. The model also predicts that the total steady-state lubricant depletion is a function of the peak ABS pressures, a statement, which needs experimental validation.

We note that in equations (2-3), p_{dis} is a nonlinear function of h. This makes the equation (1) a non-linear conservative hyperbolic partial differential equation, which has to be solved using iterative schemes such as fixed point iterations or Newton's method and makes the calculation of the lubricant profile time intensive.

Other models for flow in thin films can also be used ([7,12]) which yield different fluxes than that obtained by the continuum formulation (Equation (2-3)). However, the nature of the partial differential equation obtained does not change, although the complexity may vary depending upon the type of nonlinearity introduced in the equation. For exact modeling of observed phenomena such as lubricant modulation these formulations may have to be used and coupled with the CMLAir dynamic simulator.

Section II: Partial Contact Regime

Experiments

In this set of experiments a TTi spinstand was used to conduct touchdown-takeoff tests because the spindle rpm of this spinstand could be controlled very accurately. During each test the rpm of the disk was linearly decreased until the slider came into contact with the disk and it was increased again linearly and symmetrically until the slider ceased to be in contact with the disk. A detailed account of these tests can be found in [13,14]. An AE sensor was used to detect the contact and a Laser Doppler Vibrometer (LDV) was used to monitor the slider dynamics.

Touchdown-takeoff tests are a controlled way to study partial contact since the duration of slider-disk contact is restricted to the time between the touchdown and takeoff. These tests were conducted on INSIC disks (rms roughness 0.2 nm) with SG lubricant with 50% bonded ratio.

The CML pico 7nm design slider was flown at 0° skew over disks with three different lubricant thicknesses (0.8nm, 1.2nm and 2.0nm). After the tests the disks were scanned by OSA to determine the change in the disk lubricant due to slider-disk contact. (The calibration constant for the SG lubricant was determined to be -0.063%/nm.)

Results:

By analyzing the experimental data it was found that slider in contact with the disk could cause lubricant depletion, buildup, redistribution or modulation. It was also seen that the depletion and buildup due to intermittent slider-disk contact was much more than what was observed in the case of no contact. This might be expected as the slider-

lubricant interaction is much more intense during slider-disk contact as compared to when the slider is flying on the disk without contact.

Fig. 14(a) shows a track on a disk with 2.0 nm lubricant on which a touchdown-takeoff test was conducted. The black boxes show the regions where angular averaging was done individually to obtain cross-sections as shown in Fig. 14(b-*). In all these figures the OSA reflectivity data is shown on the left and the corresponding lubricant profile obtained from calibration is shown on the right. We notice that an increase in reflectivity corresponds to lubricant depletion, while a drop in reflectivity corresponds to lubricant buildup. It is seen that the profiles are very different from each other even though they correspond to the same track. Such a pronounced difference is not seen in the non-contact case, and is a major difference between slider-lubricant interaction in non-contact vs. the partial contact regime. In the non-contact regime it was seen that the cross-section was fairly uniform for a particular track.

Upon close observation of the profiles in each of the cross-sections we also see the effect of the trailing pad and the side rails on the lubricant. In Fig.14 (b-1) the trailing pad as well as both the side rails are seen to have caused lubricant depletion. There is also a small lubricant buildup near one edge of the trailing pad. Traversing through the rest of the figures in order, we see that there is also lubricant buildup due to the trailing pad and side rails.

The constant lubricant buildup near the trailing pad is thought to be an effect of slider roll as is explained later. Careful observation of Fig.14(b-2) shows a gentler depletion profile due the trailing pad on the side away from the lubricant buildup. Similarly, more depletion can be seen due to the side rail on the same side of lubricant

buildup in (b-4). In (b-6), we also see lubricant buildup due to one side rail but lubricant depletion due to the other.

These observations can be explained by the physical model shown in Fig. 15. Due to bouncing of the slider during intermittent contact depletion and buildup can occur. The bold arrows in subfigures (a), (b) and (c) show the direction of slider motion. Various small arrows in the lubricant film show the direction of lubricant flow in response to the slider motion. The profile on the right shows an estimated lubricant profile due to the lubricant flow which matches well with the experimentally observed profile.

Fig. 15(a) shows that when the slider is moving towards the disk and makes a contact the lubricant below the trailing pad and the side rails (low lying areas) is squeezed and moves laterally. It then accumulates in the pockets between the side rails and the trailing pad, causing lubricant buildup in these areas. Further, the effect of slider roll can also be seen. Due to the slider's roll one side of the trailing pad flies lower than the other. When slider-disk contact occurs the lower flying edge squeezes more lubricant causing a deeper ridge and a higher lubricant buildup. Such lubricant profiles can be seen in Figs. 14(b-2,4 and 5).

In addition to lubricant depletion the trailing pad and the side rails also experience lubricant buildup. Fig. 15(b) and (c) show two possible explanations of this phenomenon. Fig. 15(b) shows the possibility of a meniscus bridging the slider and the disk as the slider moves farther from the disk after bouncing. Another possibility is that when the lubricant is squeezed due to the downward slider motion the lubricant also moves in the on-track direction in addition to the lateral direction. Immediately after the contact the slider moves upward without squeezing the newly formed lubricant buildup. This causes

a lubricant buildup under the side rails and the trailing pad after the depletion, and it is also a possible mechanism for lubricant modulation, which was observed in addition to lubricant buildup and depletion.

Typically, substantial depletion was observed during severe slider-disk contact which could be inferred from the corresponding AE signal. However, when there was a very light contact (indicated by a slight increase in the magnitude of the AE signal from the base noise level), lubricant modulation was observed. Fig. 16 shows OSA scans (left) with the associated AE signal (right; purple and green correspond to AE and LDV signals respectively). It can be seen that the top two OSA scans show lubricant depletion/buildup with a clear increase in the AE signal during contact, while the bottom two OSA scans show lubricant modulation. As noted, we see a slight increase in the associated AE signal while the LDV signal does not show a sustained increase in slider dynamics, which does occur during severe contact. Thus this light contact does not influence the slider dynamics as much as a sustained contact.

Figs. 17 (a-c) show detailed images of such lubricant modulation for 0.8nm, 1.2nm and 2.0nm lubricant thickness disks. In all the cases two distinct modulated tracks are seen and they correspond to the trailing edge of the slider. Light tracks were also seen corresponding to the side rails (not seen in Fig17). From Figs. 17(a-c) substantial lubricant depletion and buildup are seen in the modulation. The peak-to-peak difference was about 0.9nm for a 2.0nm disk (45%). Frequency analysis (FFT) of the lubricant modulation profiles was done and the results are shown in Fig. 18. For the data acquisition of the lubricant profile using the OSA, the disk was rotating at a constant speed of 5000 rpm and the sampling frequency was 0.34 MHz. Hence the Nyquist

frequency was 170 KHz. In all the FFTs, strong suspension modes were observed, which are between 1-20 KHz. The highest frequency seen is about 35KHz in Fig.18(a) and (c). Since the disk rpm was varied during the touchdown-takeoff tests, the rpm at which lubricant modulation occurred is unknown. Hence, it is difficult to determine which of the suspension modes correspond to the observed frequencies. If the modulation rpm is known, then the plotted frequencies could be scaled as:

$$f_{actual} = \frac{RPM_{\mathrm{mod}ulation}}{RPM_{OSA}} \times f_{observed} \tag{7}$$

where, RPM_{OSA}= 5000, used for data acquisition of lubricant profile. Alternatively, if the observed frequency can be attributed to some particular modal frequency of the suspension, the modulation rpm can be determined.

Fig. 19(a) and (b) show the LDV signal and its FFT during light slider-disk contact respectively. We see that only the suspension modes are dominant in the slider dynamics during bouncing as they have much smaller stiffness compared to the slider modes. The dominant frequencies seen are ~77Hz, 1.52KHz and 2.15 KHz. 1.52 KHz is the first bending mode of the suspension and matches well with FEM analysis [15]. The lowest mode corresponds to the disk runout and shifts with the disk rpm. Finally, 2.15 KHz is believed to be a bending mode as the high buildup peaks and depletion valleys (dark and golden bands, respectively) in Fig. 17 under the trailing pad are in phase with each other indicating that the torsion mode of the suspension is not dominant.

Discussion:

By monitoring the condition of the disk lubricant while conducting touchdown-takeoff tests, we can obtain information about slider-lubricant interactions during partial

contact. It is seen that these interactions are more severe than in the non-contact regime. The non-uniformity in lubricant profile along the track direction is also more pronounced in partial contact regime.

Modeling of slider-lubricant interactions during partial contact is challenging as it requires accurate modeling of the lubricant flow along with a good contact model to predict the slider motion during partial contact and a dynamic slider-disk-suspension model to include the effect of suspension and disk dynamics along with the slider dynamics.

Lastly, it should be noted that although the lubricant is different than Zdol, it is expected that the qualitative results would translate to Zdol or other lubricants since the slider-lubricant interaction is much more intense during slider-disk contact as compared to when the slider is flying on the disk without contact. Because of this, the lubricant properties may not influence the interaction as much as they do in the case of no slider-disk contact. Also, the change in lubricant profile is expected to be more pronounced for untextured disks and for disks with more mobile lubricant since the lubricant can flow more easily in these cases.

Conclusions

In this report, we investigated the slider-lubricant interactions in non-contact and partial contact regimes. The main conclusions are as follows:

(a) A method is presented to include the effect of lubricant in static ABS simulations. Lubricant depletion under a flying slider was measured using the OSA and also calculated using different disjoining pressure models. Inclusion of such lubricant

depletion profiles in static simulations did not change the flying attitude of the slider appreciably. A case of severe lubricant depletion was examined and some change was seen in the slider flying attitude.

(b) Study of slider-lubricant interactions in the partial contact regime is important as the slider flying height is reduced to achieve the goal of higher areal density. From the experiments it was concluded that a slider in partial contact with the disk causes lubricant depletion, buildup, modulation or simply redistribution of the lubricant. The slider's trailing pad and side rails have an effect on lubricant depletion and buildup and so does the slider roll. Further, lubricant modulation occurs during light contact while lubricant buildup and depletion is seen when there is considerable slider-disk contact. The frequency analysis of lubricant modulation shows mainly suspension bending modes.

Acknowledgements:

The authors would like to thank Dr. Singh Bhatia and Dr. Robert Waltman of Hitachi GST for helpful discussions and for providing some of the disks used for this work. RPA would also like to thank Brendan Cox for his helpful advice. This work was supported by the Computer Mechanics Laboratory at the University of California, Berkeley, USA and the Information Storage Industry Consortium's EHDR Program.

References:

[1] X. Ma, J. Chen, H. J. Richter, H. Tang and J. Gui, "Contribution of Lubricant Thickness to Head-Media Spacing," *IEEE Trans. Magn,* Vol. 37, Vol. 4,1824-26, July 2001.

[2] T. Watanabe, D.B. Bogy, "A study of the lubricant displacement under a flying head slider caused by slider-disk interaction," *IEEE Trans. Magn.*, vol.39, no.5, pt.2, pp. 2477-9, Sept. 2003.

[3] Q. Dai, F. Hendriks and B. Marchon, "Modeling the Washboard Effect at the Head/Disk Interface," *IEEE Trans. Magn.*, Vol. 39, No. 5, pp. 2459-61, Sept. 2003.

[4] A. Khurshudov and R.J. Waltman, "The contribution of thin PFPE lubricants to slider-disk spacing," *Tribol. Lett.*, vol. 11, pp. 143-49, 2001.

[5] B. Marchon, T. Karis, Q. Dai and R. Pit, "A Model for Lubricant Flow from Disk to Slider," *IEEE Trans. Magn.*, Vol. 39, No. 5, 2447-49, Sept. 2003.

[6] B. V. Derjaguin and N. V. Churaev, "On the Question of Determining the Concept of Disjoining Pressure and its Role in the Equilibrium and Flow of Thin Films," *J. Coll. Interface Sci.*, Vol. 66, No. 3, Oct. 1978.

[7] T.E. Karis and G.W. Tyndall, "Calculation of Spreading Profiles for Molecularly-Thin Films from Surface Energy Gradients," *J. Non-Newtonian Flu. Mech.*, Vol. 82, pp. 287-302, 1999.

[8] J. Israelachvili, *Intermolecular and Surface Forces*, Academic Press, San Diego, 1992.

[9] K. Fukuzawa, J. Kawamura, T. Deguchi, H. Zhang and Y. Mitsuya, "Measurement of Disjoining Pressure of a Molecularly Thin Lubricant Film by Using a Microfabricated Groove," *IEEE Trans. Magn.*, Vol. 40, No. 4, July 2004.

[10] R.J. Waltman, A. Khurshudov and G.W. Tyndall, "Autophobic Dewetting of Perfluoropolyether Films on Amorphous Nitrogenated Carbon Surfaces," *Trib. Lett.*, Vol. 12, No. 3, pp. 163-69, Apr. 2002.

[11] M. Smallen and H.W. Huang, "Effect of Disjoining Pressure on Disk-to-Head Lubricant Transfer," *IEEE Trans. Magn.*, Vol. 39, No. 5, 2495-97, Sept 2003.

[12] A. Oron, S.H. Davis, S.G. Bankoff, "Long Scale Evolution of Thin Liquid Films," *Rev. Modern Phys.*, Vol. 69, No. 3, pp. 1-50, July 1997.

[13] R.P. Ambekar, V.Gupta and D.B. Bogy, "Experimental and numerical investigation of the dynamic instability in the head-disk interface at proximity," *ASME J. Tribol.*, vol. 127, no. 3, pp. 530-36, July 2005.

[14] R.P. Ambekar and D.B. Bogy, "Effect of Slider Lubricant Pickup on Stability at the Head-Disk Interface," *IEEE Trans. Magn.*, vol.41, no.10, Oct. 2005, pp. 3028-30.

[15] H.M. Gross, *Off-Track Vibrations of the Read-Write Heads in Hard Disk Drives*, Ph.D. dissertation, University of California-Berkeley, Spring 2003.

Tables

Model	1nm		2nm	
	Max (nm)	Min (nm)	Max (nm)	Min (nm)
1	1.05	0.7	2.8	0.8
2	1.25	0.85	2.02	1.72
3A	1.01	0.88	2.01	1.88
3B	1.02	0.82	2.02	1.82
3B/10	1.2	0	2.2	0.2

Table 1: Maximum and minimum lube height predicted by different models for original lube thicknesses of 1nm and 2nm.

		Nominal FH (nm)	Pitch (rad)	Roll (rad)	Peak pressure (atm)	Lube Height (below transducer) (nm)
CML Pico	Before	5.250	289.468	-2.105	8.5243	1.2
	Model2	5.246	289.478	-2.108	8.5243	0.9704
	Expt	5.241	289.453	-2.104	8.5246	1.13
CML Femto	Before	5.930	286.789	5.437	14.1207	1.2
	Model2	5.931	286.789	5.435	14.1213	0.8797
	Expt	5.920	286.671	5.408	14.1102	1.0368

Table 2: Comparison between static simulation results with and without the effect of lube depletion

		Nominal FH (nm)	Pitch (rad)	Roll (rad)	Peak pressure (atm)	Lube Height (below transducer) (nm)
CML Pico	Before	6.046	289.478	-2.108	8.5287	2
	After	5.861	289.555	-2.106	8.6767	1.3491
HD Pico	Before	14.752	125.549	1.809	20.6463	2
	After	14.608	125.021	1.821	20.6473	0
CML Femto	Before	6.730	286.789	5.437	14.1207	2
	After	6.628	285.663	5.419	14.3801	0.0393
DSI Femto	Before	8.080	214.798	-11.386	11.7261	2
	After	7.863	213.027	-11.297	12.1436	0.5072
HD Femto	Before	18.431	146.871	2.533	17.8183	2
	After	18.337	146.026	2.549	17.8005	0.1132

Table 3: Static simulation results for different ABS designs to show maximum effect of lube depletion on the flying attitude of the slider.

Figures:

Section I

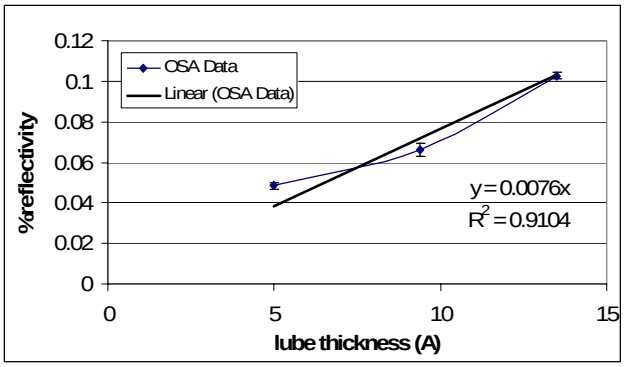

Figure 1: OSA Calibration for Zdol 4000

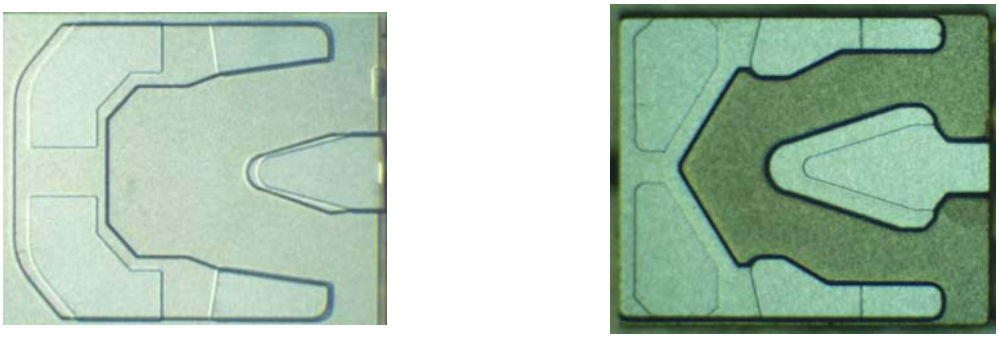

(a) (b)

Figure 2: ABS designs used for experiments: (a) CML Pico 7nm; (b) CML Femto 3.5nm

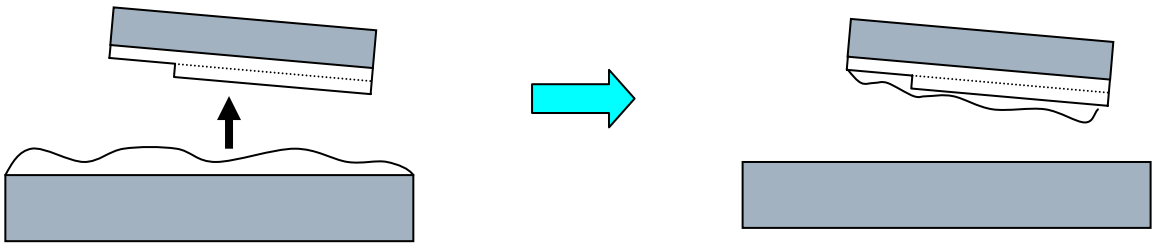

Figure 3: Adding the lube profile on the disk to the slider

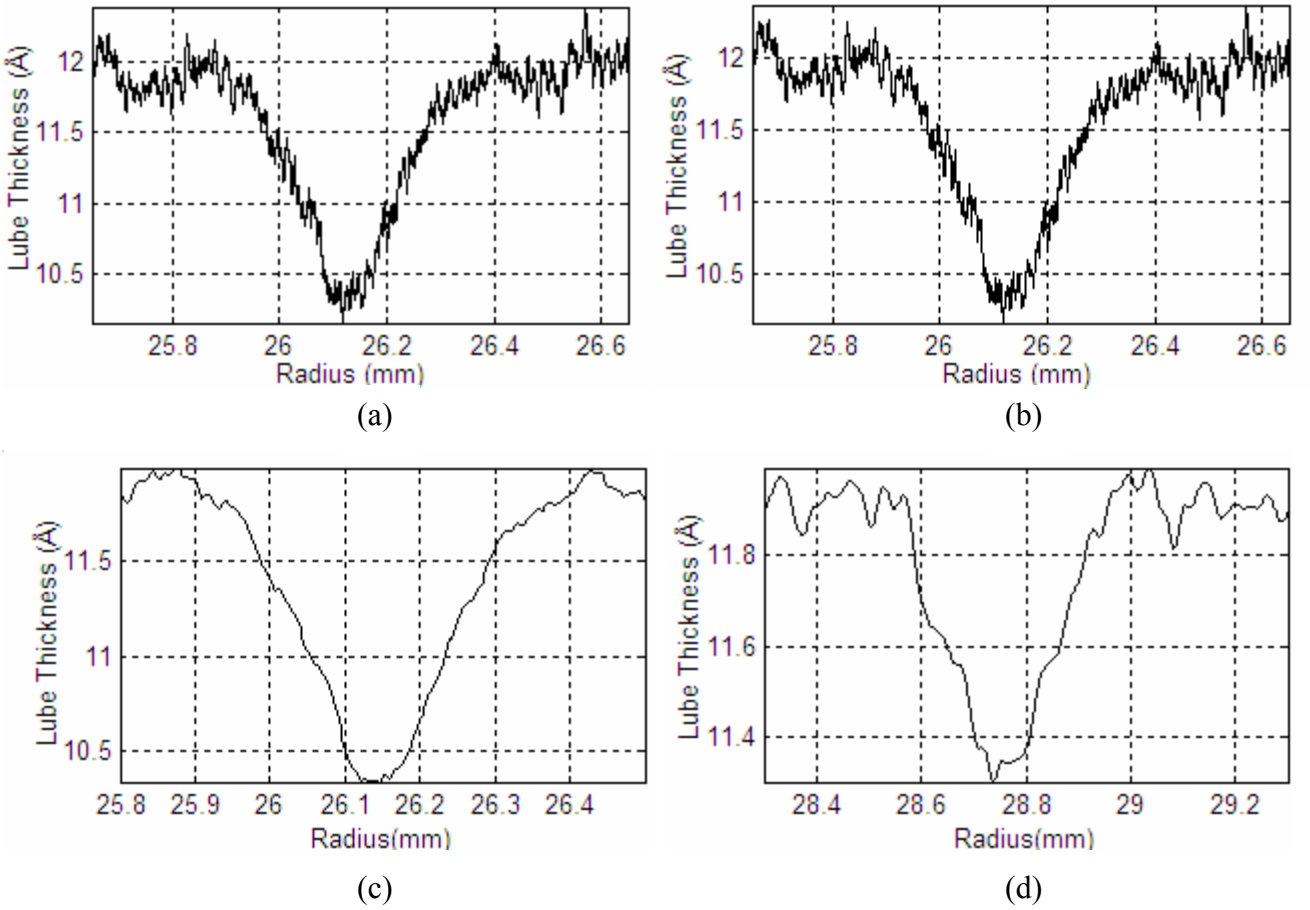

Figure 4: Experimentally measured lube profiles: (a) Lube depletion for CML Femto after 15mins; (b) Lube depletion for CML Femto after 30mins; (c) Lube profile used for CML Femto static simulations, obtained from (b) after smoothing; (d) Lube profile used for CML Pico simulations

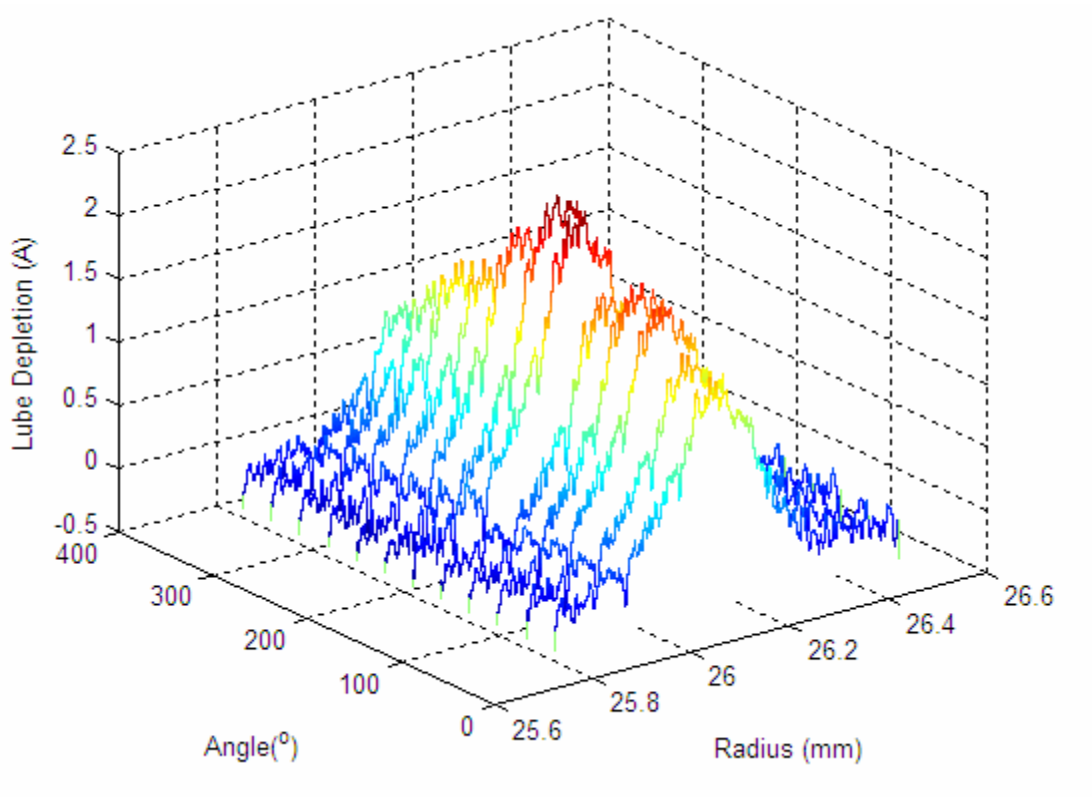

Mean (Peak Depletion) = 1.75 Å
Stdev (Peak Depletion) = 0.39 Å

Figure 5: Waterfall plot of cross-section of lube profile at various angles along the circumferential direction for showing uniformity in lube depletion.

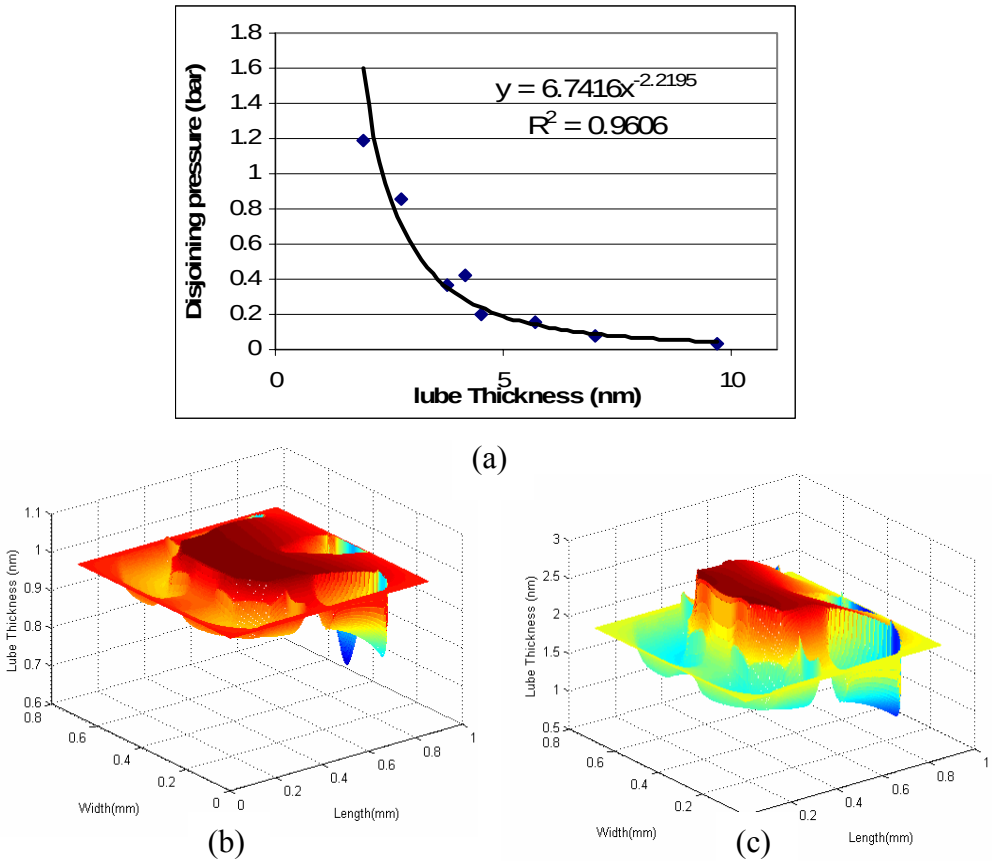

Figure 6: Model 1 used for predicting lube depletion: (a) Data fit to experimental measurements of disjoining pressure [9]; (b) Lube profile for 1nm thick lube with CML Pico slider; (c) Lube profile for 2nm thick lube with CML Pico slider

Note: CML Pico slider also used for lube profiles in Figs. 8-10.

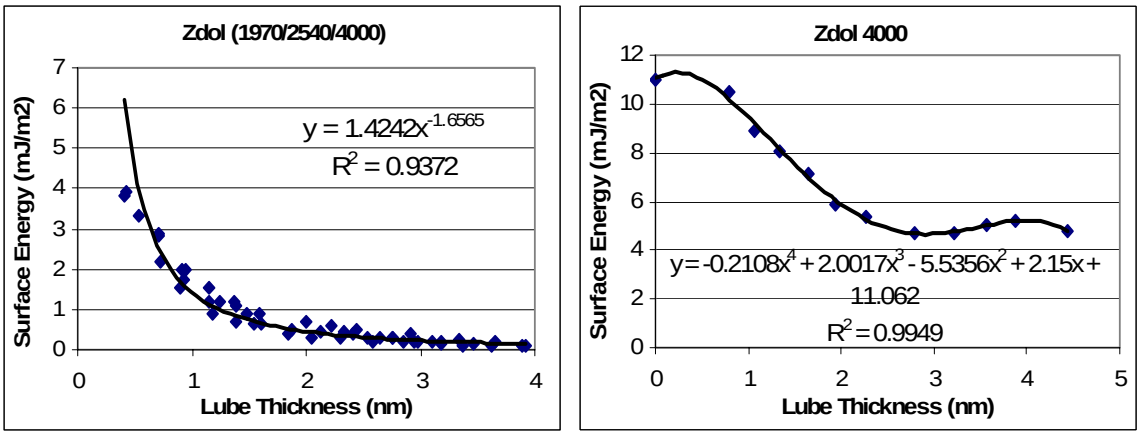

(a) (b)

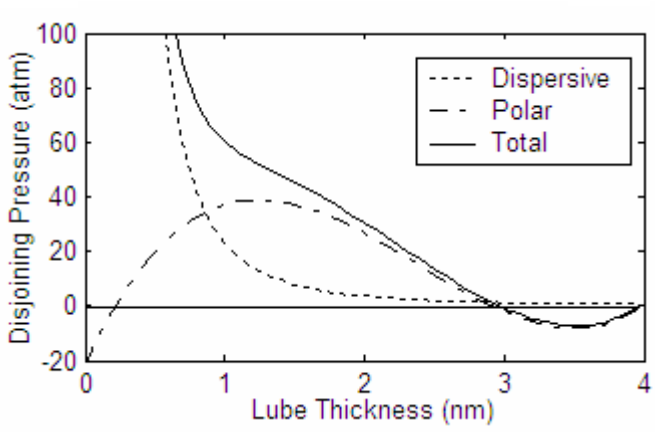

$$p_{dis}^{d} = 23.24\ h^{-2.646}\ (atm)$$

$$p_{dis}^{p} = 8.31\ h^{3} - 59.16\ h^{2} + 109.08\ h\ -21.1823\ \ (atm)$$

(c)

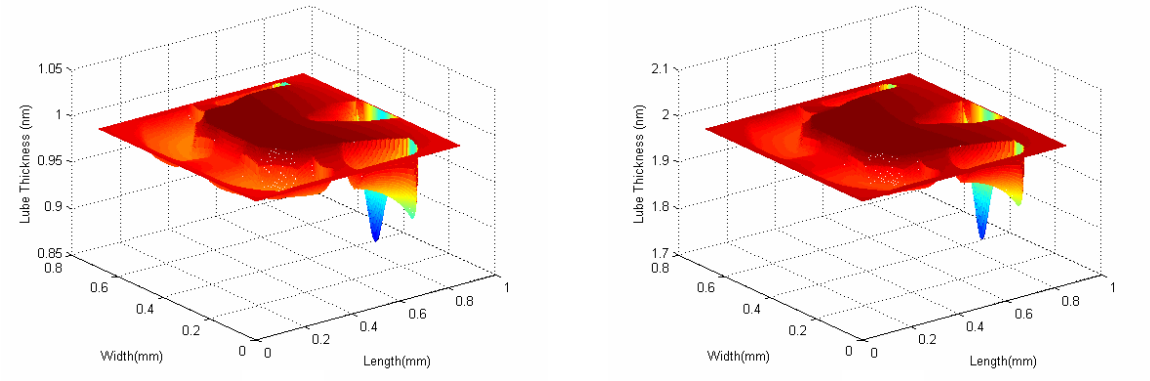

(d) (e)

Figure 7: Model 2 used for predicting lube depletion: (a) Data fit to experimental measurements of dispersive surface energy [10]; (b) Data fit to experimental measurements of polar surface energy [10]; (c) Plot of polar, dispersive and total disjoining pressure using data fits obtained from (a) and (b); (d) Lube profile for 1nm thick lube; (e) Lube profile for 2nm thick lube

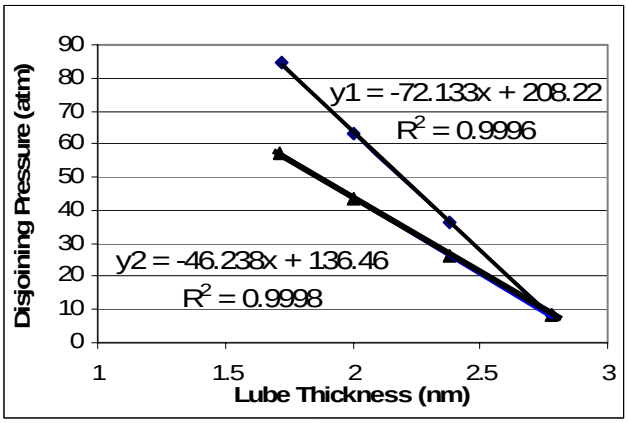
Disjoining Pressure (atm)
Lube Thickness (nm)
y1 = -72.133x + 208.22
R2 = 0.9996
y2 = -46.238x + 136.46
R2 = 0.9998

(a)

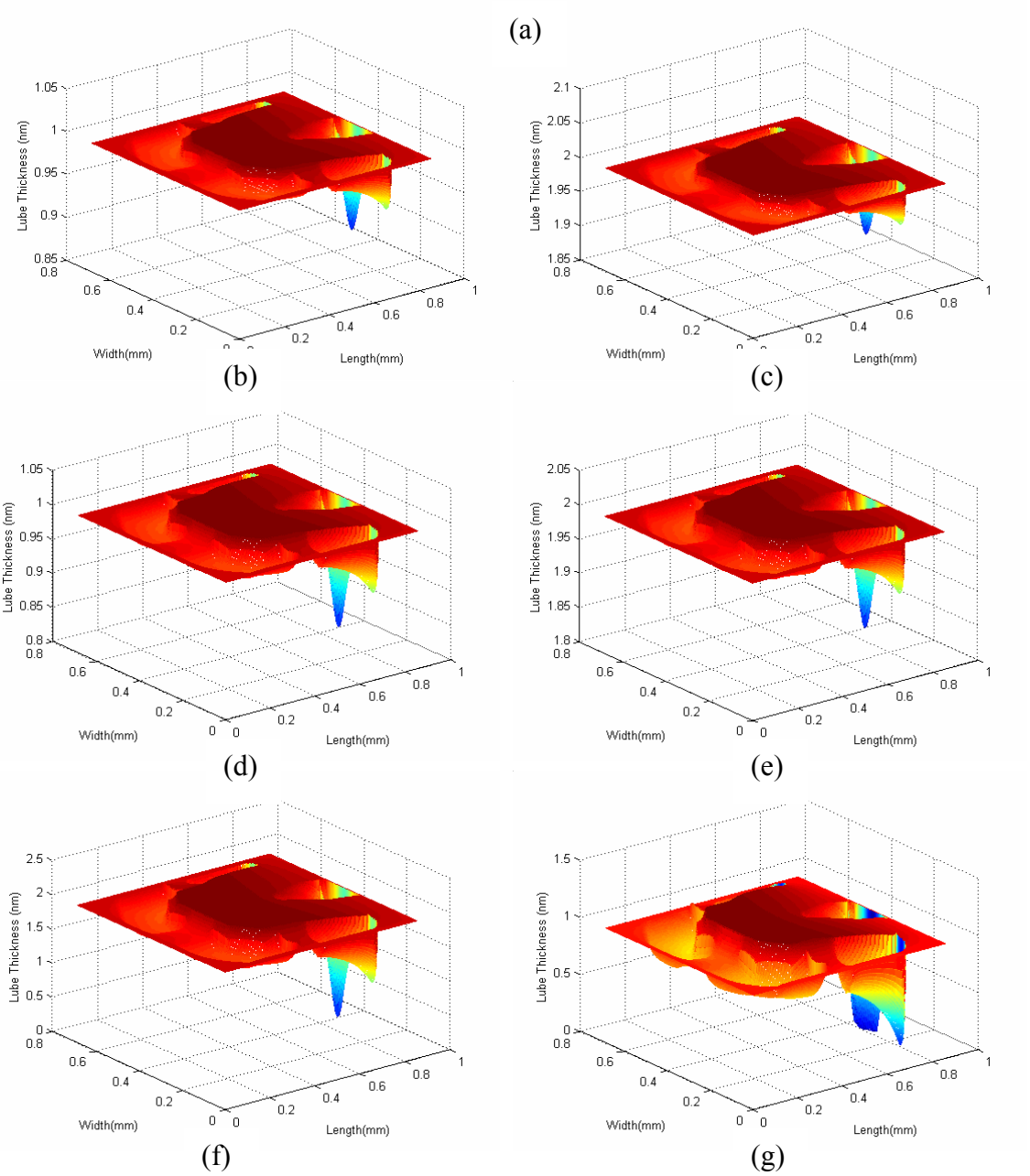
Lube Thickness (nm)
Width(mm)
Length(mm)

(b) (c)

(d) (e)

(f) (g)

Figure 8: Model 3 used for predicting lube depletion: (a) Data fits to experimental measurements of disjoining pressure [11]. Black and blue lines correspond to models 3A and 3B respectively; (b) Lube profile for 1nm thick lube using model 3A (c) Lube profile for 2nm thick lube using model 3A; (d) Lube profile for 1nm thick lube using model 3B (e) Lube profile for 2nm thick lube using model 3B; (f) Lube profile for 1nm thick lube using model 3B/10; (g) Lube profile for 2nm thick lube using model 3B/10

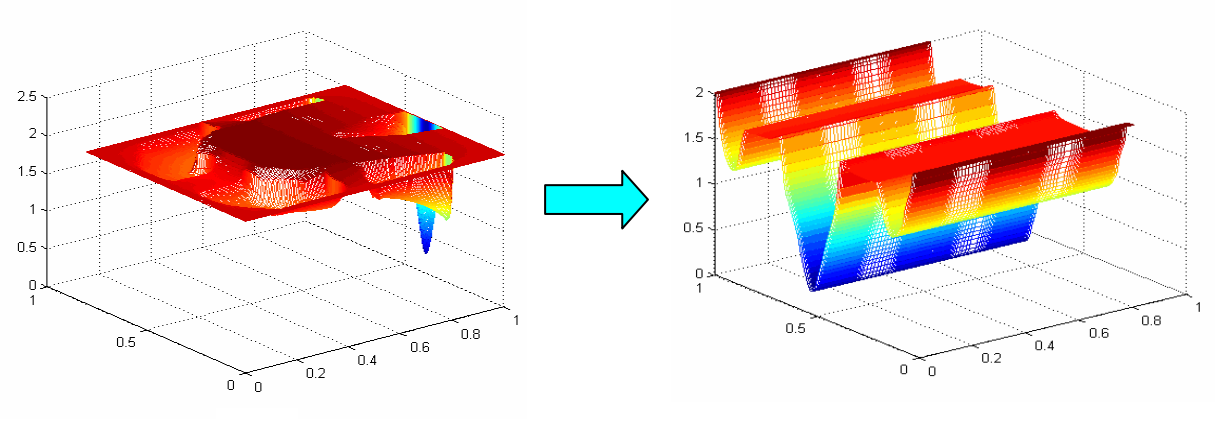

Figure 9: Extruding the lube profile: (a) Lube profile estimated by model 2; (b) Extruded lube profile added to slider profile for static simulations

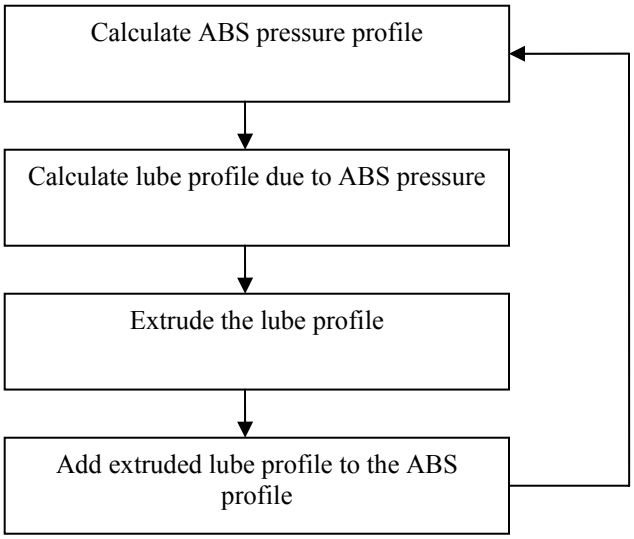

Figure 10: Algorithm for static simulations for inclusion of the effect of lube

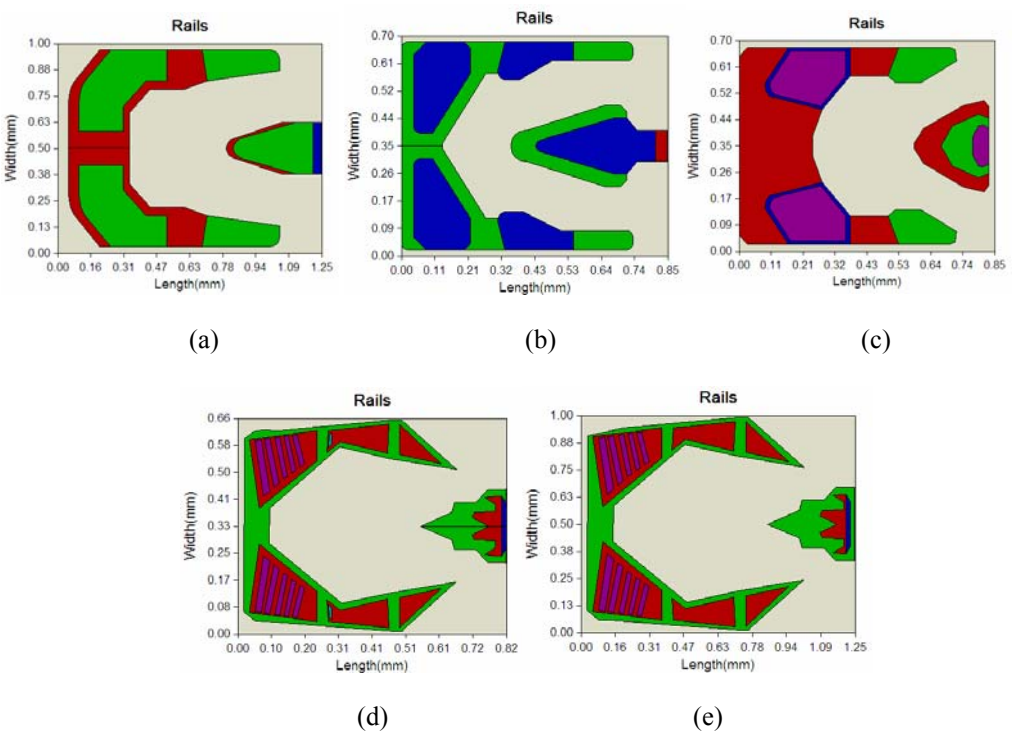

Figure 11: ABS designs used for simulations: (a) CML Pico; (b) CML Femto; (c) DSI Femto; (d) High Damped (HD) Pico; (e) HD Femto

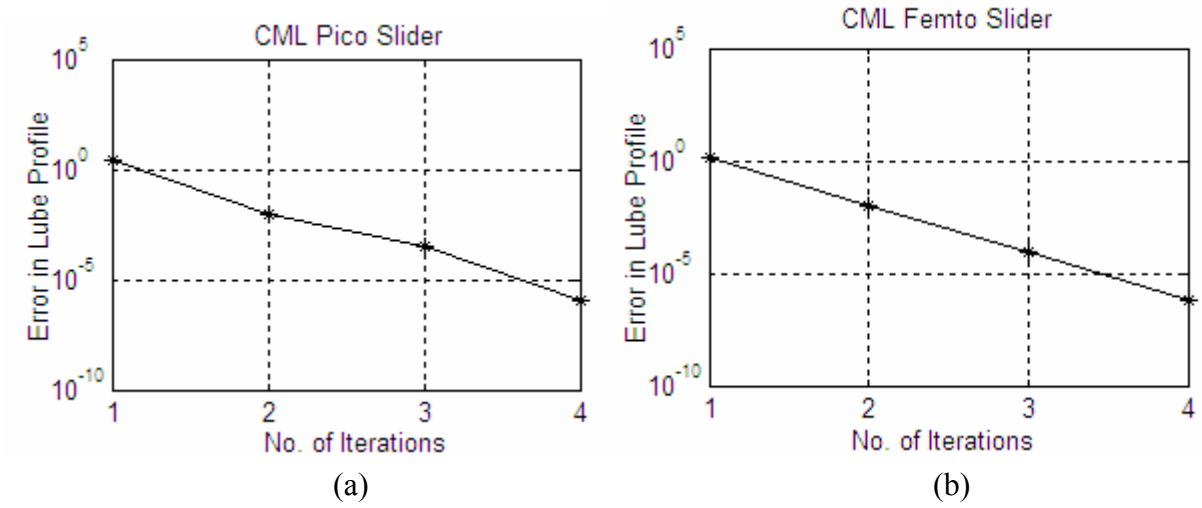

Figure 12: Convergence for simulation procedure outlined in Figure 10; (a) Convergence for CML Pico slider; (b) Convergence for CML Femto slider

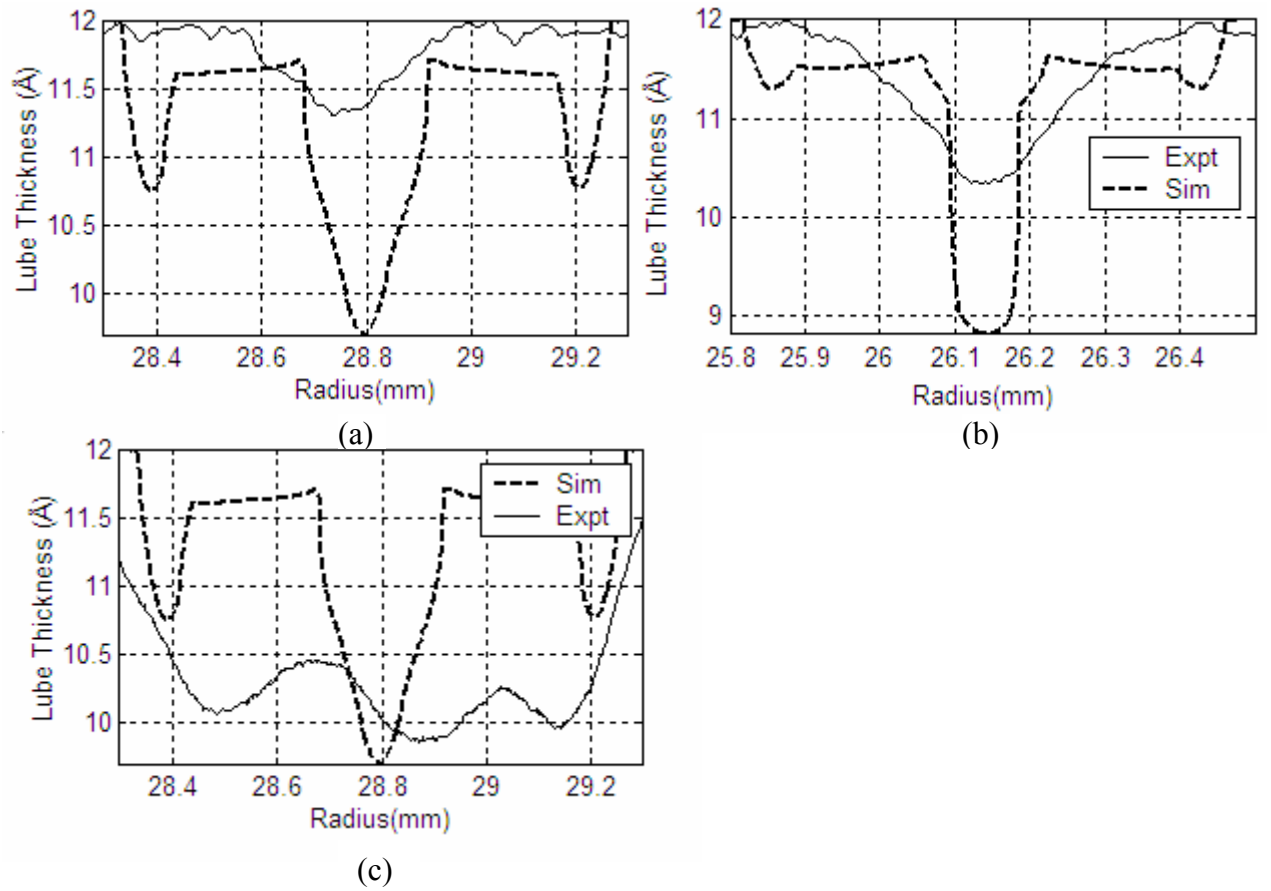

Figure 13: Comparison between experimental and numerical lube profile: (a) For CML pico slider ; (b) For CML Femto slider; (c) One of the observed profiles for CML pico slider, lacked circumferential uniformity.

Section 2:

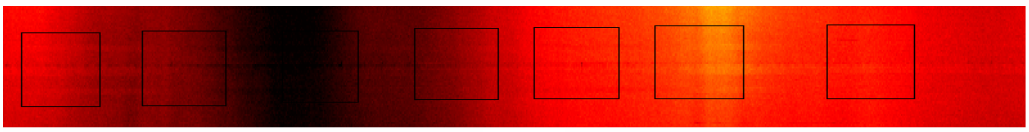

(a)

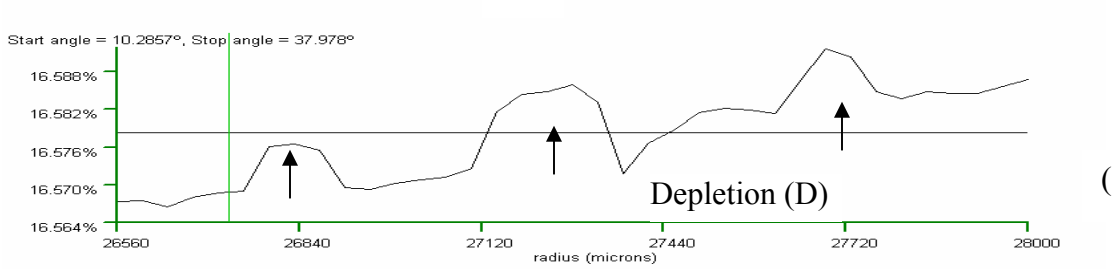

(1)

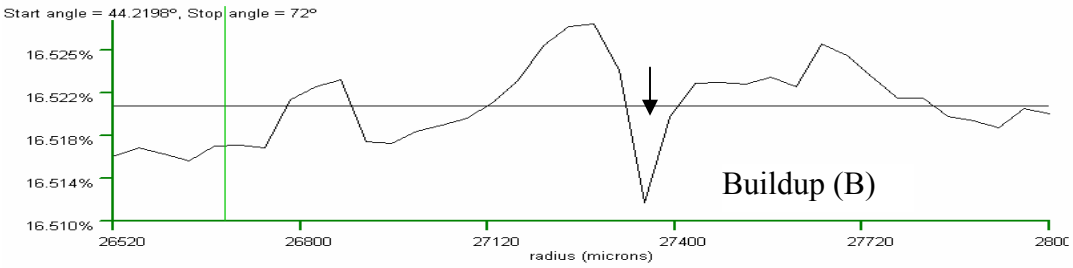

(2)

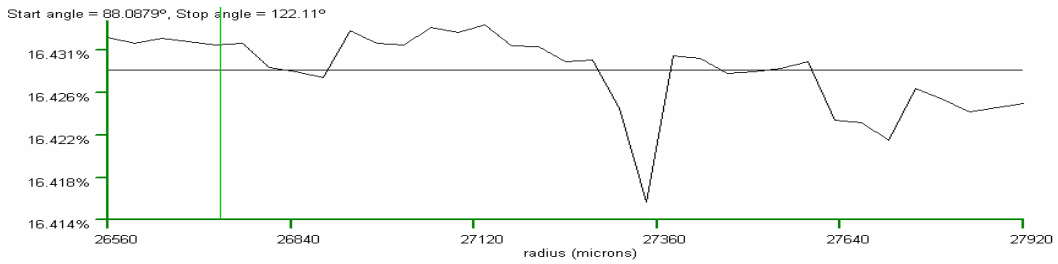

(3)

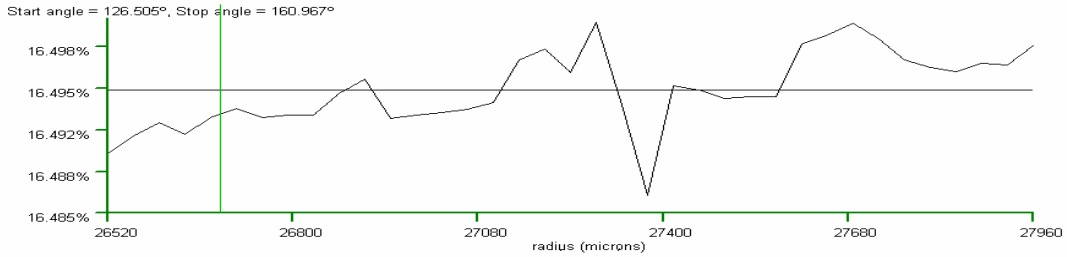

(4)

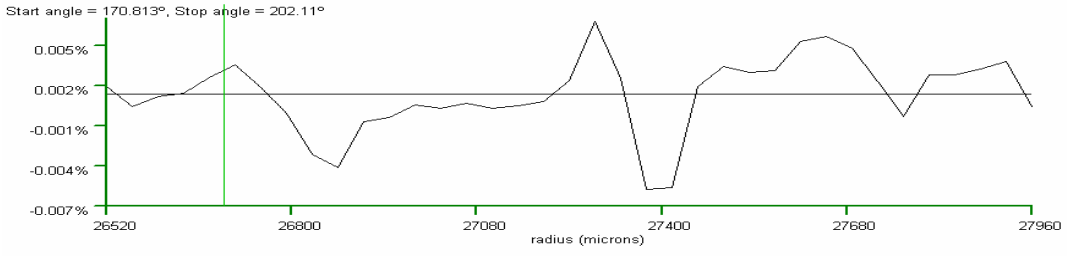

(5)

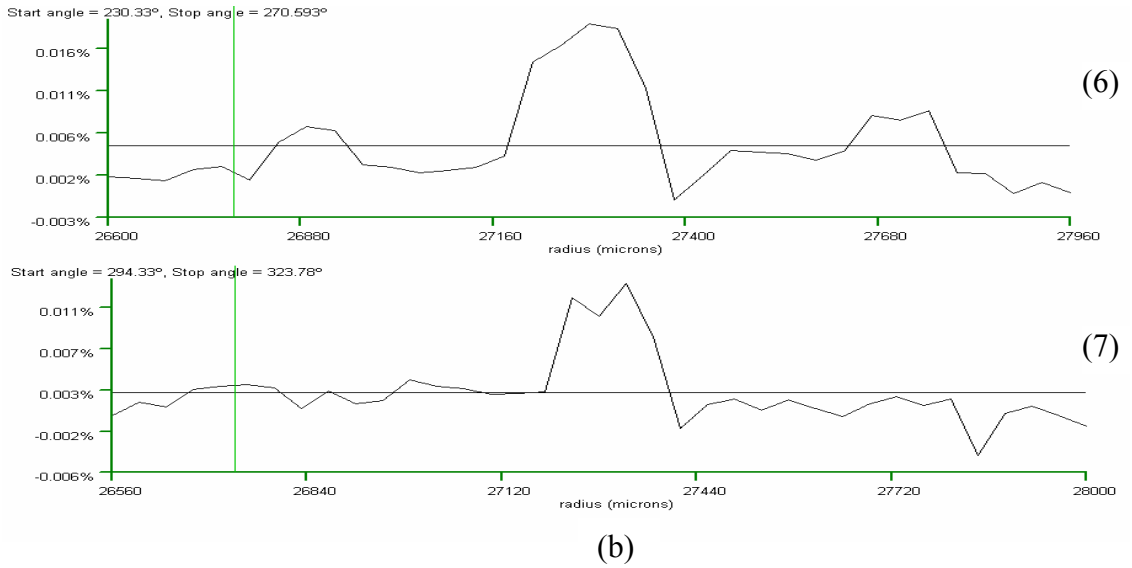

(b)

Figure 14: Lubricant profile as a result of slider-disk partial contact: (a) OSA scan of the experimental track; (b) Lubricant profiles corresponding to each of the black squares in (a).

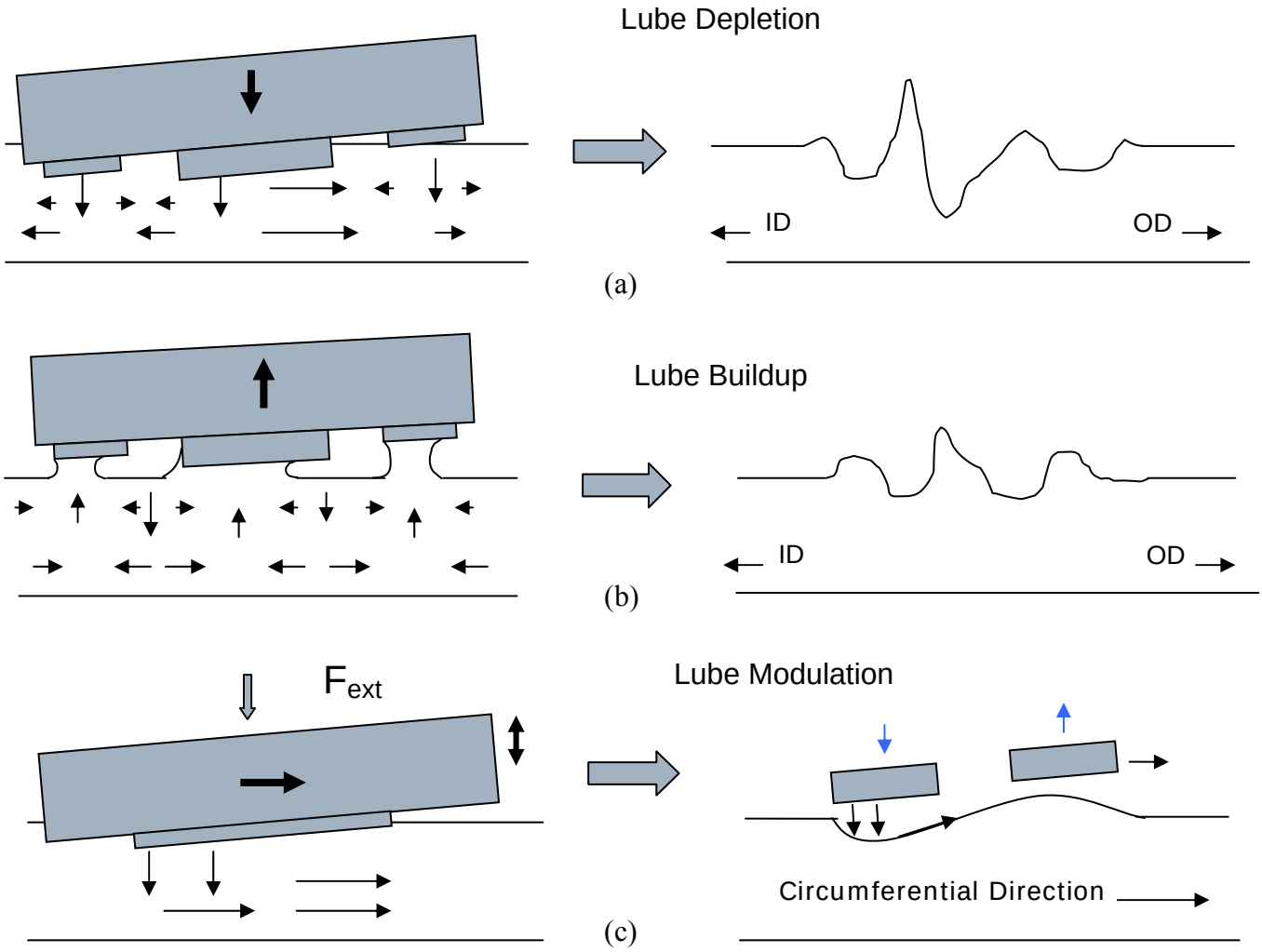

Figure 15: Physical explanation for experimentally observed lube profiles during slider-disk partial contact: (a) Lube depletion due to downward motion of the slider; (b) Lube buildup due to upward motion of the slider; (c) Lube modulation due to bouncing of the slider

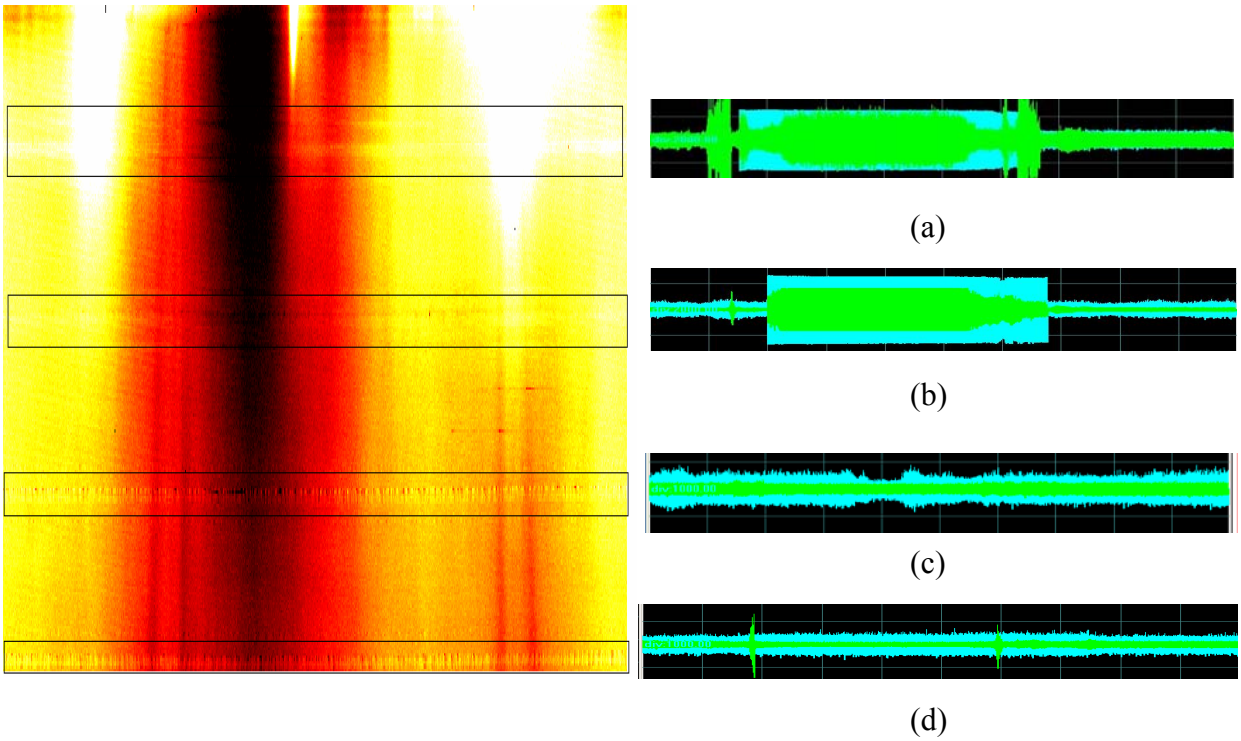

Figure 16: AE(blue) and LDV (green) signals with corresponding lube profile observed during experiments: (a) and (b) Lube depletion observed when substantial slider-disk contact; (c) and (d) Lube modulation observed when light slider-disk contact.

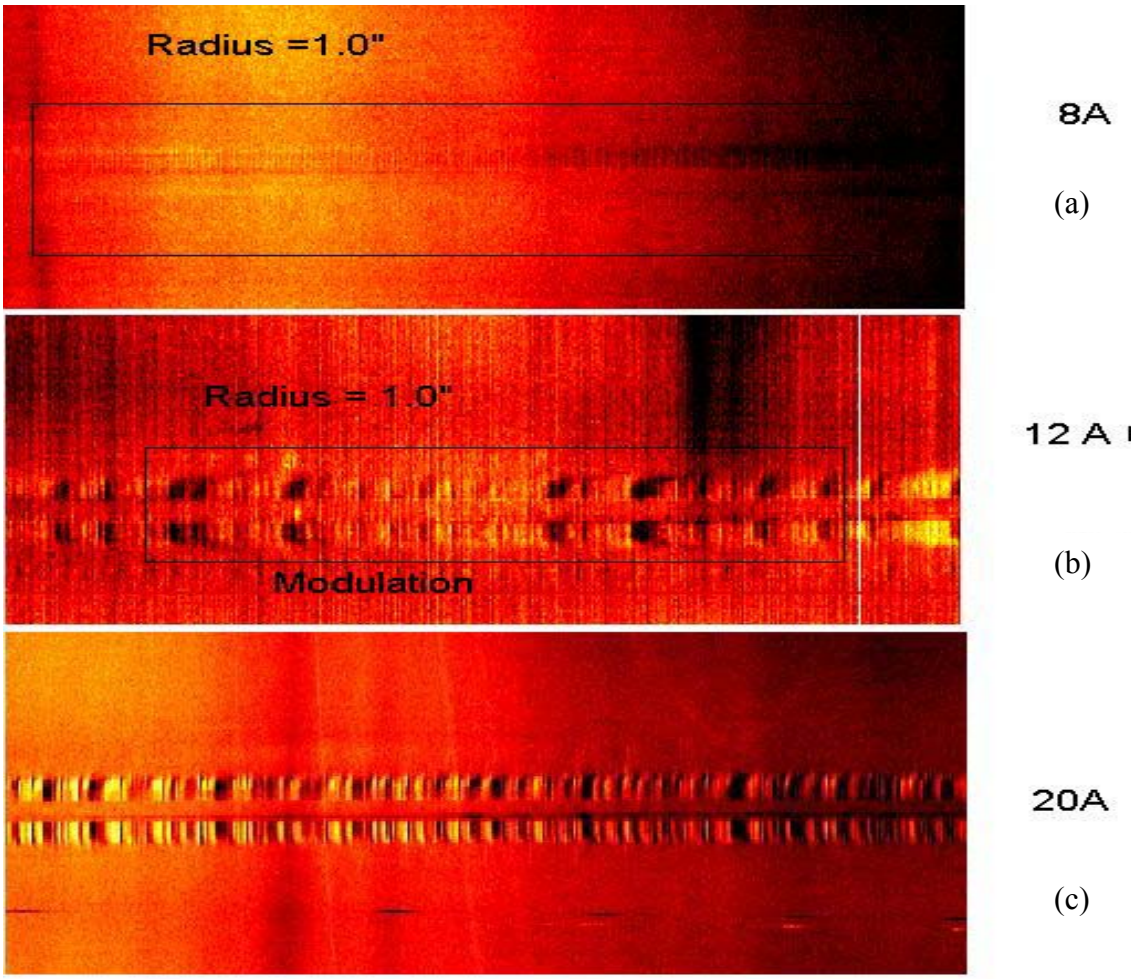

Dark bands in modulation correspond to lubricant buildup and light/golden bands correspond to lube depletion

8A: Max P-P buildup/depletion = 0.030% ~ 5 Å
12A: Max P-P buildup/depletion = 0.035% ~ 6 Å
20A: Max P-P buildup/depletion = 0.055% ~ 9 Å

Figure 17: Lube modulation under slider trailing pad observed for disks with different lube thicknesses

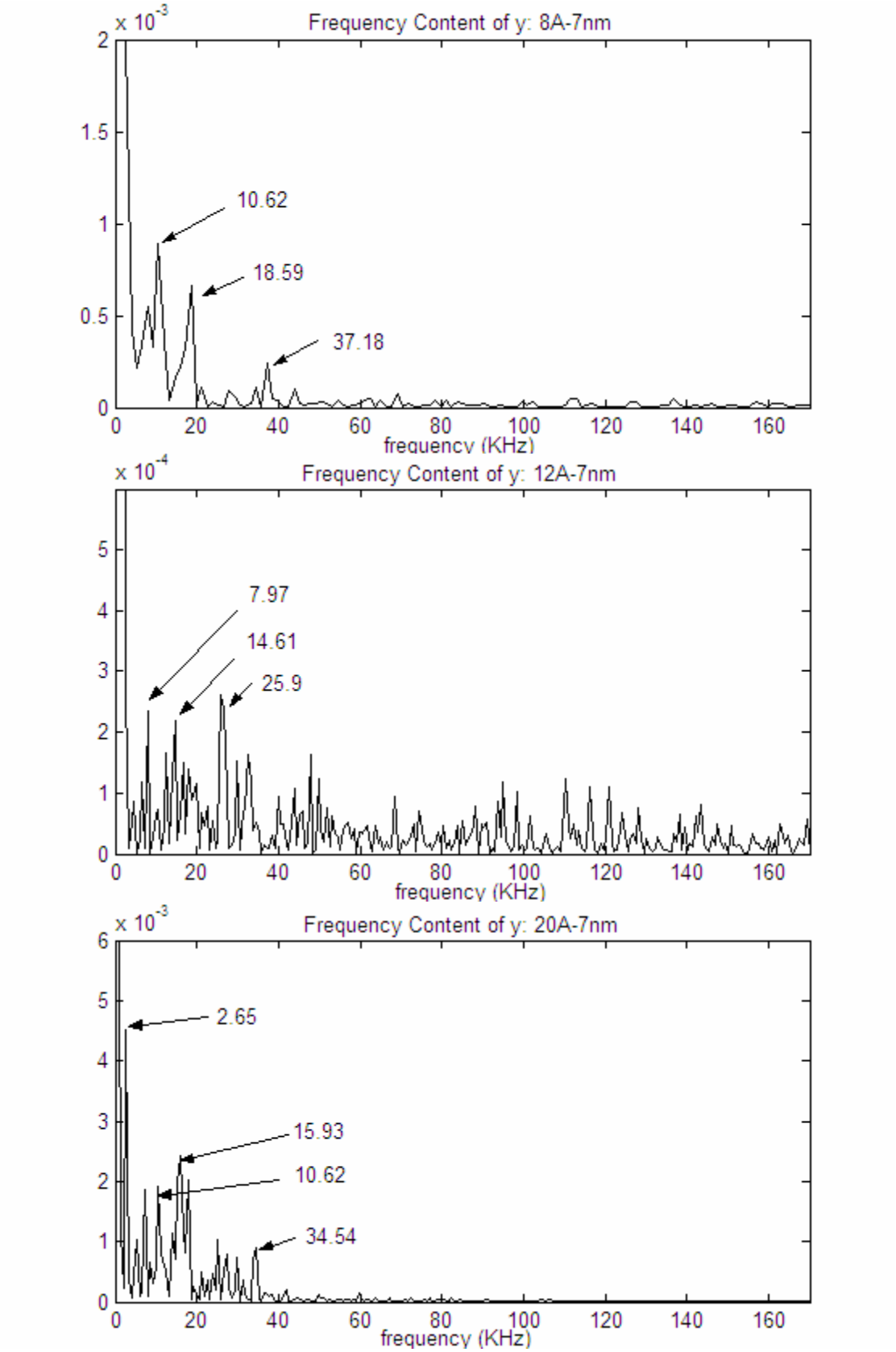

Figure 18: Frequency content of lube modulation for (a) 8Å; (b) 12Å and (c) 20Å disks

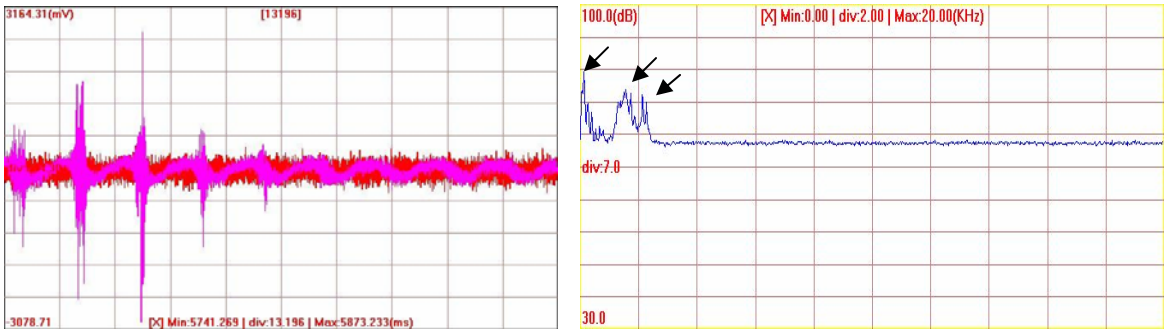

(a) (b)

Figure 19: Slider dynamics corresponding to observed lube modulations: (a) Time history during light contact; (b) Frequency content during light contact